

1  
2  
3  
4  
5  
6  
7  
8  
9  
10  
11  
12  
13  
14  
15  
16  
17  
18  
19  
20  
21  
22  
23  
24

# Satellite derived trait data slightly improves tropical forest biomass, NPP and GPP predictions

Christopher E. Doughty\*<sup>1</sup>, Camille Gaillard<sup>1</sup>, Patrick Burns<sup>1</sup>, Yadvinder Malhi<sup>2</sup>, Alexander Shenkin<sup>1</sup>, David Minor<sup>4</sup>, Laura Duncanson<sup>4</sup>, Jesus Aguirre-Gutierrez<sup>2</sup>, Scott Goetz<sup>1</sup>, Hao Tang<sup>5</sup>

<sup>1</sup>School of Informatics, Computing, and Cyber Systems, Northern Arizona University, Flagstaff, AZ, USA

<sup>2</sup>Environmental Change Institute, School of Geography and the Environment, University of Oxford, Oxford, UK

<sup>3</sup>Department of Biology, Northern Arizona University, Flagstaff, AZ, USA

<sup>4</sup>Geographical Sciences, University of Maryland College Park, Maryland , USA

<sup>5</sup>Department of Geography, National University of Singapore, Singapore

\*to whom correspondence should be addressed – [chris.doughty@nau.edu](mailto:chris.doughty@nau.edu)

**Keywords** –GEDI, tropical forests, traits, LMA, biomass

25

26 **Abstract**

27 Improving tropical forest biomass predictions can accurately value tropical forests for their  
28 ecosystem services and establish confidence in carbon trading schemes such as REDD+. Optical  
29 remote sensing estimates of tropical forest biomass have produced spatially contradictory results  
30 that differ from ground plot biomass data. Recently, the Global Ecosystem Dynamics  
31 Investigation (GEDI) lidar was activated on the international space station (ISS) to improve  
32 biomass predictions by providing detailed 3D forest structure and height data. However, there is  
33 still debate on how best to predict tropical forest biomass using GEDI data. Here we compare  
34 GEDI predicted biomass to 2,102 tropical forest biomass plots and find that adding a remotely  
35 sensed (RS) trait map of LMA (Leaf Mass per Area) significantly ( $P < 0.001$ ) improves field  
36 biomass predictions, but by only a small amount ( $r^2 = 0.01$ ). However, it may also help reduce the  
37 bias of the residuals because, for instance, there was a negative relationship between both LMA  
38 ( $r^2$  of 0.34) and % P ( $r^2 = 0.31$ ) and residuals. This improvement in predictability corresponds  
39 with measurements from 523 individual trees where LMA predicts Diameter at Breast height  
40 (DBH) (the critical measurement underlying plot biomass) with an  $r^2 = 0.04$ , and spectroscopy  
41 (400-1075 nm) predicts DBH with an  $r^2 = 0.01$ . Adding environmental datasets may offer further  
42 improvements and max temperature ( $T_{\max}$ ) predicts Amazonian biomass residuals with an  $r^2$  of  
43 0.76 ( $N = 66$ ). Finally, for a network of net primary production (NPP) and gross primary  
44 production (GPP) plots ( $N = 21$ ), RS traits are better at predicting fluxes than structure variables  
45 like tree height or Height Of Median Energy (HOME). Overall, trait maps, especially future  
46 improved ones produced by surface biology geology (SBG), may improve biomass and carbon  
47 flux predictions by a small but significant amount.

48

## 50 Introduction

51 In an era of rapid climate change, accurately predicting forest carbon stocks is  
52 increasingly important because carbon stored in forests can potentially offset anthropogenic  
53 emissions that cause climate change. For this reason, international climate agreements such as  
54 REDD+ (Reducing Emissions from Deforestation and Degradation) have been developed to  
55 encourage countries to conserve their forests. Using forests as natural climate change solutions,  
56 by incentivizing carbon trading and offset schemes, requires accurate and repeatable  
57 measurements of forest aboveground biomass (AGB) (CEOS, 2014, Goetz et al., 2015). Earth  
58 observation satellite remote sensing (RS), coupled with ground-based measurements, have the  
59 potential to provide systematic estimates of AGB over vast spatial extents. Therefore, much  
60 effort has been put into developing such maps of AGB, albeit with mixed results. For instance,  
61 two remotely sensed biomass maps showed markedly different biomass trends from each other  
62 and from 413 ground plots (Baccini et al., 2012; Mitchard et al., 2014; Saatchi et al.,  
63 2011)(Avitabile et al., 2016). Mitchard et al 2014 found the uncertainties were actually > 25%  
64 more than those listed in the RS maps of Baccini et al 2012 and Saatchi et al 2011 (Mitchard et  
65 al., 2013, 2014). They advise to incorporate basal area-weighted wood density estimates and note  
66 that depending only on the relationships between tree height and biomass may lead to large,  
67 spatially correlated errors. Partially in response to such difficulties in predicting biomass with  
68 optical RS, the Global Ecosystem Dynamics Investigation (GEDI) Lidar mission was launched  
69 and installed on the International Space Station (ISS) in late 2018 and operational products  
70 started in March 2019 (R. Dubayah et al., 2020). GEDI is the first spaceborne lidar designed for  
71 terrestrial ecosystem research and the first specifically developed to accurately measure forest  
72 canopy 3D structure. However, converting from laser energy returns to accurate biomass  
73 predictions is not trivial.

74 GEDI covers most land areas below 52 degrees latitude, but it does not provide wall to  
75 wall coverage and gaps between GEDI tracks are greatest at tropical latitudes owing to the  
76 orbital configuration of the ISS. To develop pre-launch calibrated models of AGB, ground  
77 biomass plots were combined with coincident aircraft lidar data using a waveform simulator  
78 (Hancock et al., 2019) to produce the GEDI Level-4A (footprint level) algorithm (Duncanson et  
79 al., 2022). Currently the L4A product for tropical forests uses relative height (RH) 98 and RH 50  
80 to predict a median Above Ground Biomass (AGB) of 300 Mg Ha<sup>-1</sup> for tropical forests (0.66 r<sup>2</sup>  
81 and RMSE of 10.4). Duncanson et al. (2022) compares these results to previous studies. For  
82 instance, Asner and Mascaro (2014) used a network of 804 field inventory plots and aircraft  
83 discrete return lidar in 5 tropical countries to estimate biomass with a R<sup>2</sup> = 0.92 and RMSE =  
84 17.1 Mg/ha. Saatchi et al. (2011) combined several datasets with a Maximum Entropy  
85 modelling framework across the Tropics to get an r<sup>2</sup> of 0.80 and RMSE= 23.8. Baccini et al.  
86 (2012) used GLAS (Global Laser Altimetry System) on IceSat-1 together with image data from  
87 MODIS (MODerate resolution Imaging Sensor) across the Tropics in a modelling framework of  
88 ordinary least squares regression and random forest machine learning algorithms with predictors  
89 of HOME (Height of Median Energy), other Height Metrics, and total Canopy returned energy to  
90 get an r<sup>2</sup> of 0.83 and RMSE= 22.6. These early studies exemplify the wide variety of techniques  
91 and accuracies used to predict biomass in tropical forests. Forest structure data products derived  
92 from GEDI are also related to AGB. For instance, Doughty et al 2023 found forest stratification  
93 (% of forests with only one peak in PAVD (Plant Area Volume Density) versus those with

94 several peaks) correlated with biomass more strongly than tree height (Doughty et al., 2023).  
95 Duncanson et al 2022 used algorithms stratified by 4 plant functional types and 6 world regions  
96 but did not include other remotely sensed (e.g. optical image) data as predictor variables for  
97 biomass. Here we explore the extent to which incorporating external datasets and having more  
98 regional calibrations can improve GEDI biomass predictions across tropical forests.

99 Environment (e.g., soils and climate) influences the community assembly of tropical  
100 forests and knowing species composition could improve biomass estimates since different  
101 species have different wood density and structure. For instance, Amazonian plant biogeography  
102 may follow a south-west/north-east soil fertility gradient and a north-west/south-east  
103 precipitation gradient (ter Steege et al., 2006). Soil cation concentrations are the primary driver  
104 of floristic variation for Amazonian trees (Tuomisto et al., 2019) with climate being of secondary  
105 importance. However, in central African forests, climate is considered to be the driving factor of  
106 floristic patterns (Réjou-Méchain et al., 2021). Therefore, inclusion of soils or forest floristic  
107 maps could improve biomass predictions.

108 Leaf traits may also improve tropical forest biomass predictions. One global study of  
109 plant traits found that three-quarters of trait variation is captured in a two-dimensional global  
110 spectrum of plant form and function (Díaz et al., 2016). One major dimension within this plane  
111 reflects the size of whole plants and their parts; the other represents the leaf economics spectrum,  
112 which balances leaf construction costs against growth potential (Díaz et al., 2016). Since the size  
113 of whole plants may reflect their biomass, there are leaf traits correlated with plant size and  
114 structure that may prove predictive. Traits, such as foliar chemical content, like nitrogen (N),  
115 and morphological traits, like leaf mass area (LMA), can be predicted remotely using high-  
116 resolution leaf (Asner & Martin, 2008)(Homolová et al., 2013) and canopy (Asner et al.,  
117 2016)(Cawse-Nicholson et al., 2021) spectroscopy (400-2500nm) and algorithms based on  
118 partial least squares (PLS) regression or other machine learning statistical techniques. Spectral  
119 properties can even predict chemicals not directly expressed in the spectrum, such as base  
120 cations or phosphorus (P) because these chemicals have stoichiometric relationships with  
121 chemicals that are expressed spectrally (Ustin et al., 2006). Other tree traits such as wood  
122 density can be predicted with spectroscopy, i.e. traits that are not directly expressed in leaf  
123 spectra but that are instead correlated with leaf traits such as LMA (Doughty et al., 2017). Wall  
124 to wall trait maps for leaf chemistry, leaf thickness ( $r^2 = 0.52$ ) leaf carbon content ( $r^2 = 0.70$ ) and  
125 maximum rates of photosynthesis ( $r^2 = 0.67$ ) have recently been created using Sentinel-2 spectral  
126 data, soils and environmental data (Aguirre-Gutiérrez et al., 2021).

127 Gross primary production (GPP) and Net Primary Production (NPP) are also important  
128 fluxes to calculate, but currently are not accurately predicted for tropical forests. For instance,  
129 Cleveland et al 2015 compared tropical NPP estimates from field-based methods, RS methods  
130 (like MODIS) and mechanistic model-based methods (like CLM). The three methods had similar  
131 estimates of NPP (i.e.,  $\sim 10 \text{ Mg C yr}^{-1}$ ), but displayed differing patterns of NPP through space  
132 and through time. The RS based methods to predict NPP made limited use of RS spectral data  
133 and relied more on climate based inputs. We are approaching the era of Surface Biology and  
134 Geology (SBG) an upcoming wall to wall hyperspectral satellite) (Cawse-Nicholson 2021;  
135 Schimel & Poulter, 2022) with hopes for accurate wall to wall trait maps of tropical forests.

136 For this paper we focus on the extent to which plant trait data may help to improve  
137 predictions of tropical forest biomass and fluxes. We start by using a large trait database to  
138 explore whether traits can predict individual tree DBH. Next, we compare GEDI predicted  
139 biomass to field plot biomass and examine how well RS derived trait maps predict field and RS  
140 biomass. Finally, we determine the extent to which structure and traits can improve predictions  
141 of tropical forest carbon fluxes (NPP and GPP). We test the following hypotheses:

142 *H1 - Leaf spectral and trait data can predict tree diameter (DBH), the main variable in*  
143 *predicting biomass.*

144 *H2 - Leaf traits and environmental data will improve predictions of both field and GEDI*  
145 *biomass.*

146 *H3 - GEDI structure or RS trait maps will improve NPP or GPP predictions.*

147

148

## 149 **Materials and Methods**

150 **Field leaf trait and spectroscopy data** - We used leaf trait and spectral data from an extensive  
151 field campaign along an elevation gradient (from 3500 m to 220 m elevation) in the Peruvian  
152 Amazon where leaf traits for 60-80% of basal area of trees >10cm DBH were measured within a  
153 well-studied 1 ha plot network from April – November 2013 (Enquist et al., 2017). In each one  
154 ha plot (N=10 plots), we sampled the most abundant species as determined through basal area  
155 weighting (enough species generally to cover ~80% of the plot's basal area). For each species,  
156 we sampled the five (three in the lowlands) largest trees (based on diameter at breast height  
157 (DBH)) and sampled one sun and one shade branch. On each of these branches, leaf chemistry  
158 and leaf mass area (LMA) was measured with methodology detailed in Asner et al. (2014). On  
159 five randomly selected leaves for each branch, we measured hemispherical reflectance with an  
160 ASD Fieldspec Handheld 2 with fiber optic cable, contact probe which has its own calibrated  
161 light source and a leaf clip (Analytical Spectral Devices High Intensity Contact Probe and Leaf  
162 Clip, Boulder, Colorado, USA) following (Doughty et al., 2017). We measured leaf  
163 spectroscopy (400-1075 nm) on the same branches where the leaf traits were collected. Both  
164 LMA and Chlorophyll A had previously been shown with this dataset to have a correlation with  
165 leaf spectroscopy (Doughty et al., 2017). However, we had not previously tried to compare leaf  
166 spectral data with DBH directly.

### 167 **Plot data** –

168 *Aboveground biomass* - We used 2,102 of 19,160 total AGB field plots between +30° and -30°  
169 latitude classified as broadleaf evergreen trees by MODIS PFT using public data from  
170 Duncanson et al 2022 that was organized and publicly available through ORNL DAAC as an  
171 RDS (R data serialization) file. Distribution of plots are shown in Fig S1 (AGB) and S2  
172 (residuals).

173 *NPP and GPP* - We also used 21, 1 ha plots where NPP and sometimes GPP were measured  
174 following the GEM protocol (Malhi et al., 2021). We focused on two regions: a Peruvian  
175 elevation transect with both NPP + GPP (n= 10, RAINFOR plot codes are ALP11, ALP30,  
176 SPD02, SPD01, TRU03, TRU08, TRU07, ESP01, WAY01, ACJ01(Malhi et al., 2017)) and a  
177 Bornean logging transect with only NPP (n= 11 RAINFOR plot codes are DAN-04, DAN-05,  
178 LAM-01, LAM-02, MLA-01, MLA-02, SAF-01, SAF-02, SAF-03, SAF-04, SAF-05 (Riutta et  
179 al., 2018). These plots were chosen because there are large changes in NPP/GPP across the  
180 elevation or logging gradient.

181 **GEDI data** – We used the vertical forest structure (L2A and L2B, Version 2) and biomass (L4a)  
182 products from the GEDI instrument (R. Dubayah et al., 2020) between April 2019 to December  
183 2022 for tropical forest regions (R. O. Dubayah et al., 2023). We used a quality filtering recipe  
184 developed in collaboration with GEDI Science Team members from University of Maryland and  
185 NASA Goddard to identify the highest quality GEDI vegetation shots (R. Dubayah et al.,  
186 2022). A data layer that this iterative local outlier detection algorithm uses to exclude data is  
187 publicly available at (R. O. Dubayah et al., 2023). For instance, some of the key data filters we  
188 applied were: included degrade flags of 0,3,8,10,13,18,20,23,28,30,33,38,40,43,48,60,63,68,  
189 L2A and L2B quality flags = 1 (only use highest quality data), sensitivity >= 0.98. With the

190 GEDI data we used canopy height, height of median energy (HOME), and the number of canopy  
191 layers following Doughty et al 2023 (Doughty et al., 2023).

192 Across all tropical forests, we created 300 by 300 m pixels containing all averaged  
193 (mean) GEDI data between 2019 and 2022. Using the centroid coordinates from each of the  
194 2,102 plots, we found the 300 by 300 m averaged GEDI pixel that encompassed the plot. If the  
195 plot was not encompassed by the GEDI data, we searched a wider area by incrementally  
196 averaging a gradually increasing area of 1, 3, 5, and 10 pixels. In other words, if no 300 by 300  
197 m pixel encompassed the plot, then we averaged all GEDI data an area one pixel out (4 by 4 =  
198 1200 by 1200 m, 6 by 6 = 1800 by 1800m, 11 by 11 = 3300m by 3300m), gradually increasing  
199 the square until it encompassed an area with GEDI data. To compare with the NPP/GPP plots  
200 we compared RS trait and GEDI data for individual footprints within a 0.03 km radius of the plot  
201 coordinates.

202  
203 **Remotely sensed leaf trait data** - Based on a broader set of field campaigns, Aguirre-Gutiérrez  
204 et al., (2021) used Sentinel-2, climatic, topography and soil data to create remotely sensed  
205 canopy trait maps for P=phosphorus % leaf concentration, WD = wood density  $\text{g}\cdot\text{cm}^{-3}$ , and  
206 LMA=Leaf mass area  $\text{g}\cdot\text{m}^{-2}$ .

207 **Other data layers** – We compared % one peak to several other climate, soils, leaf traits, and  
208 ecoregion maps listed below for the Amazon basin. Each dataset had its own resolution, which  
209 we standardized to 0.1 by 0.1 degrees. We used total cation exchange capacity (CEC) from soil  
210 grids (Batjes et al., 2020) from 0-5cm in units of  $\text{mmol}(c)/\text{kg}$ . We averaged TerraClimate  
211 (Abatzoglou et al., 2018) data between 2000 and 2018 for Vapor Pressure Deficit (VPD in kPa),  
212 Mean Monthly Precipitation (MMP) (mm/month), potential evapotranspiration (PET) and  
213 maximum and minimum temperature ( $^{\circ}\text{C}$ ).

214 **Statistical analysis** –We used the matlab (Matlab, MathWorks Inc., Natick, MA, USA) function  
215 “fitlm” to fit linear models to compare variables such as soils data, environmental data, leaf trait  
216 data (at  $0.1^{\circ}$  resolution) and GEDI structure data (300m and bigger resolution) to field biomass  
217 and NPP/GPP estimates. The P values listed are for the *t*-statistic of the two-sided hypothesis  
218 test. We used R to create a linear model to predict the best model ranked by AIC and parsimony  
219 using the dredge function from the MuMIn library(Bartoń, 2009). We also used CAR package  
220 (Fox J & S, 2019) and the VIF command to test for multi-collinearity between variables. To  
221 account for spatial autocorrelation, we used Simultaneous Auto-Regressive (SAR<sup>err</sup>) models (F.  
222 Dormann et al., 2007) using the R library ‘spdep’ (Bivand, Hauke, & Kossowski, 2013). We  
223 tested different neighborhood distances from 10 km to 300 km and found that AIC was  
224 minimized at 80 km (Fig S3) and the corresponding correlogram showed reduced spatial  
225 autocorrelation (Fig S4). To predict leaf traits with the spectral information, we used the Partial  
226 Least Squares Regression (PLSR) (Geladi & Kowalski, 1986) using the PLSregress command in  
227 Matlab (Matlab, MathWorks Inc., Natick, MA, USA). To avoid over-fitting the number of latent  
228 factors we minimized the mean square error with K-fold cross validation. We use 70% of our  
229 data to calibrate our model and then the remaining 30% to test the accuracy of our model using  
230  $r^2$ . We use adjusted  $r^2$  which penalizes for small sample sizes throughout the manuscript.

231

232 **Results**

233 We compared averaged trait values collected from cut branches to the DBH of that tree for 3695  
234 leaves from 523 trees (Doughty et al., 2017) along a Peruvian elevation gradient which exhibited  
235 a low correlation ( $r^2 < 0.01$ ) between leaf chemistry (N and P) and DBH. However, LMA showed  
236 a significant ( $P < 0.0001$ ) positive correlation with DBH and Chlorophyll A showed a significant  
237 ( $P < 0.0001$ ) negative correlation but with relatively low variance explained ( $r^2 \sim 0.04$  and  $0.06$   
238 respectively) (Figure 1). LMA had a significant ( $P < 0.0001$ ) negative correlation with tree height  
239 ( $r^2 \sim 0.17$ ). We then compared tree averaged leaf spectral data (400 to 1075 nm) to DBH using  
240 the PLSR technique and found only a weak correlation (Figure 2,  $r^2 = 0.01$ ). LMA is predictable  
241 with spectroscopy ( $r^2 = 0.63$ ) and DBH is weakly predictable with LMA ( $r^2 = 0.04$ ), and this  
242 translated into spectra being able to predict DBH with an  $r^2 = 0.01$  in this dataset.

243 We then compared predictions of GEDI biomass to 2,102, 25m (although some 1 ha) biomass  
244 plots across *all tropical forests* (not just Peru) (Fig 3). These plot data were used to create  
245 GEDI's Level 4 footprint-level AGB product using simulated waveforms from ALS collocated  
246 with field plots. In contrast, we created 300 by 300 m pixels containing all averaged (mean)  
247 GEDI data between 2019 and 2022 across all tropical forests. We acknowledge a degree of  
248 circularity in our analysis, but the comparison is different than Duncanson et al 2022 because due  
249 to the variable nature of GEDI data collection, owing to the variable ISS orbital tracks, only  
250  $\sim 45\%$  of the plots had plot data within the 300 by 300m pixel and  $\sim 2.5\%$  of the plots needed an  
251 area of 3300m by 3300m. We therefore are not aligning field and GEDI data but are instead  
252 assessing regional correlations among variables of interest, thus our expected correlations will be  
253 much lower than where GEDI and field plots are geolocated and temporally aligned. We then  
254 subtracted GEDI regional averages of predicted biomass from field derived biomass (henceforth  
255 referred to as residuals) for 2102 plots across the tropics and showed both their location, AGB,  
256 and the average difference from the GEDI predicted value (Fig 3). There are spatial patterns  
257 with the residuals with, for instance, GEDI overestimating AGB in the Yucatan Peninsula and  
258 underestimating in the Eastern Amazon. Overall, the residuals have two modes at  $\sim -100$  and  $100$   
259  $\text{Mg ha}^{-1}$ . Next, our goal is to determine whether the bias can be reduced by incorporating RS  
260 leaf traits or other external datasets.

261 For these 2,102 plots, there was a significant ( $P < 0.0001$ ) negative correlation between the  
262 remotely sensed trait of LMA for both GEDI biomass ( $r^2 = 0.38$ ) and GEDI measured forest  
263 height ( $r^2 \sim 0.43$ ) (Fig 4). There was a significant ( $P < 0.0001$ ) negative correlation between  
264 remotely sensed % P and biomass and height ( $r^2 = 0.31$  and  $r^2 = 0.36$  respectively). However,  
265 LMA predicted field derived biomass poorly ( $r^2 \sim 0.01$ ) and % P was not correlated with field  
266 derived biomass ( $P > 0.05$ ). LMA was always a stronger predictor than P concentration, for  
267 height, RS biomass and field derived biomass.

268 We then compared LMA, %P, GEDI height and % one peak to biomass residuals and found a  
269 negative relationship between LMA and residuals ( $r^2$  of  $0.34$ ,  $N=66$ ) and a negative relationship  
270 with % P ( $r^2 = 0.31$ ). Of GEDI structure variables, % one peak did poorly, only predicted 4 % of  
271 the variance but tree height predicted biomass strongly with an  $r^2$  of  $0.74$  (Figure 5). We then  
272 subset the AGB field plots for the Amazon basin ( $N=66$  of 2102 total) to match our climate and  
273 soils datasets. We compared climate data (VPD,  $T_{\text{max}}$ , PET) and soils data (cation exchange  
274 capacity - CEC) to biomass residuals and found  $T_{\text{max}}$  was best in predicting residuals with an  $r^2$



275 of 0.79 followed by PET ( $r^2=0.70$ ) and VPD ( $r^2=0.28$ ) (Figure 6). We did not find a significant  
276 relationship ( $P>0.05$ ) between CEC and biomass residuals.

277 We tested for spatial autocorrelation and found that averaging around a radius of 80 km (this  
278 large radius may incorporate broader climate trends) minimized AIC (Figure S3) which reduced  
279 spatial autocorrelation according to the correlogram (Figure S4). There was some collinearity  
280 between the trait variables and structure variables ( $VIF>3$ ), so we removed %P and HOME and  
281 this reduced all collinearity scores to under  $\sim 1.5$ . To predict RS biomass, the best model by AIC  
282 included LMA, height, and % one peak, but LMA was only marginally significant (Table 1). For  
283 field biomass, the best model by AIC again included all three variables but % one peak was not  
284 significant. After controlling for spatial autocorrelation by grouping the plot data into  
285 neighborhoods of 80km, the statistical models changed. Adding LMA (but not %P, HOME, or  
286 % one peak) significantly ( $P<0.0001$ ) improved field biomass predictions. Adding traits  
287 (neither LMA or P) did not significantly improve RS biomass but both % one peak and HOME  
288 did ( $P<0.0001$ ). Overall, canopy height was always by far the most important predictor of AGB  
289 but adding RS LMA did improve predictions of field biomass by  $\sim 0.01 r^2$ .

290 We then predicted NPP and GPP data with traits (LMA and % P) and structure (biomass, tree  
291 height, and % one peak). LMA showed the strongest correlation with both NPP ( $r^2=0.38$ ) and  
292 GPP ( $r^2=0.41$ ) (Figure 7). Tree height and % one peak were not significantly correlated with the  
293 NPP/GPP plot data. For the logging gradient in Borneo there was a significant correlation with  
294 both tree height and LMA to NPP with LMA stronger. However, when we combined the Borneo  
295 and Amazonia data sets together, only LMA remained significantly correlated with NPP (Figure  
296 8).

297

298

299

## 300 Discussion

301 After controlling for spatial autocorrelation, adding RS derived LMA trait data significantly  
302 improves predictions of field measured (but not GEDI estimated) tropical forest biomass, only by  
303 a small amount (improving  $r^2$  by  $\sim 0.01$ ) but information criteria (AIC) suggest LMA should be  
304 added. An important caveat is that we are not comparing geolocated field plot data to GEDI and  
305 trait data for the same exact area, but instead for the broader region (i.e. only 45% of the ABG  
306 plots have GEDI data within a 300 by 300m area). This differs from Duncanson et al 2022  
307 where airborne lidar data were used to simulate GEDI data for each plot, therefore comparing  
308 predicted GEDI structure for the same area as the field plots. Since there is much regional  
309 variation in biomass, our predictions of field measured biomass are very low ( $r^2 \sim 0.03$ ) but were  
310 significantly improved with RS LMA data. LMA also directly predicts field biomass with an  $r^2$   
311  $\sim 0.01$  (Figure 4). At the individual tree scale (Figure 1), we show similar results with LMA  
312 predicting 4% of DBH variance (highly correlated with biomass) and spectral properties  
313 predicting 1% of DBH variance (Figure 2). However, predicting biomass at the canopy scale  
314 may have more success than at the leaf scale, because canopies incorporate more spectral  
315 information with higher LAI (Baret et al., 1994). Therefore, we estimate that adding RS trait  
316 data to GEDI results in a real, but very small improvement in field biomass predictability, but is  
317 this meaningful? The GEDI L4A product for tropical forests currently has an accuracy of 0.66  $r^2$   
318 (Duncanson et al., 2022), so any real improvement is welcome, if real. However, adding non-  
319 GEDI data to biomass predictions could also introduce error which could cancel out the 1%  
320 improvement.

321 Some of our results tentatively suggest that adding traits could lead to a greater improvement in  
322 AGB prediction than suggested above by reducing bias in the residuals. For instance, we found  
323 the remotely sensed trait of LMA was correlated with both GEDI biomass ( $r^2=0.38$ ) and GEDI  
324 measured forest height ( $r^2 \sim 0.43$ ) (Fig 4). We also found both LMA ( $r^2$  of 0.34) and % P  
325 ( $r^2=0.31$ ) correlated with the biomass residuals. This suggests that traits could potentially  
326 correct for bias in current GEDI predictions, which could be more useful than a 0.01  
327 improvement in  $r^2$ . However, because the leaf traits maps use predictors of soils and climate data  
328 in addition to Sentinel 2 spectral data, the improvements to biomass prediction may be due to the  
329 influence of the underlying climate variables as shown in Fig 6. LMA and % P correlated more  
330 with RS AGB than field AGB possibly for this reason as well. There is optimism for future  
331 improvements in predictability because our leaf spectral data only extends through 1075 nm, and  
332 there is likely important spectral information at longer wavelengths (e.g. in the shortwave  
333 infrared). The current RS trait maps (Aguirre-Gutiérrez et al., 2021) use a few Sentinel 2  
334 spectral bands but future satellites like Surface Biology Geology (SBG) (Cawse-Nicholson 2021;  
335 Schimel & Poulter, 2022) or the Plankton, Aerosol, Cloud, ocean Ecosystem (PACE) mission  
336 (Gorman et al., 2019) will have improved or wall to wall hyperspectral data and therefore future,  
337 more accurate trait maps may improve biomass predictions by a greater amount.

338 Our strongest (non-GEDI) predictor of biomass residuals was  $T_{\max}$  with an  $r^2$  of 0.79, but we  
339 note that this is based on a much smaller Amazon only dataset ( $N=66$ ) (Fig 6). The negative  
340 correlation suggests that GEDI underpredicts biomass in regions where VPD or  $T_{\max}$  is on  
341 average higher. Stressful temperature or water conditions may reduce tree biomass and height  
342 from their maximum potential or select for smaller species with more conservative strategies.  
343 This result is supported by other literature showing higher temperatures reduce tropical forest

344 growth rates (Clark et al., 2003). Soil cation concentration was not a strong predictor of biomass  
345 residuals in our dataset which is surprising because soil cation concentrations are the primary  
346 driver of floristic variation for Amazonian trees (Tuomisto et al., 2019) with climate being of  
347 secondary importance.

348 In a previous paper, we had hypothesized that forest stratification (% one peak or the number of  
349 single stratum forests as a percentage of total) might improve biomass predictions better than a  
350 simple metric like rh50 (Doughty et al., 2023) because in that paper, % one peak predicted  
351 biomass better than tree height. Ecological theory suggests that a stratified forest with more  
352 large emergent trees is indicative of an older forest (Halle et al., 1980), which generally has  
353 higher biomass and carbon content. However, in our study, % one peak was a fairly poor  
354 predictor of the residuals explaining only 4% of the variance compared to 75% with tree height,  
355 16% with rh50 and 36% with HOME. When we added % one peak to our overall model it did  
356 not improve the AIC, and therefore seems a poor predictor of biomass across tropical forests.  
357 Moving forward, terrestrial lidar can expand our understanding of tree structure and possibly  
358 create improved biomass estimates beyond DBH (Stovall & Shugart, 2018).

359 Remotely sensed MODIS NPP and GPP is a commonly used input to many global models  
360 (Zhang et al., 2012) but previous studies have found that MODIS NPP does not match ground  
361 based estimates of NPP seasonality and therefore, there is a need for improved remote sensed  
362 NPP estimates (Cleveland et al., 2015). Our results (Fig 7 and 8) suggest that adding trait maps  
363 to predictions of GPP and NPP could potentially improve accuracy, but GEDI structure metrics  
364 did not improve predictability. For instance, remotely sensed LMA predicted GPP ( $r^2=0.4$ ) and  
365 NPP ( $r^2=0.35$ ) better than GEDI height in an Andean elevation gradient (Fig 7). When we  
366 combined both datasets, only LMA continued to predict NPP (Fig 8). However, although we  
367 used the biggest NPP and GPP dataset in the tropics, our sample size ( $N=21$ ) was small. More  
368 ground based NPP/GPP networks are necessary for validation before we would have confidence  
369 in this result.

370 Overall, we find adding RS trait maps may slightly improve predictions of tropical forest  
371 biomass and fluxes and may be further improved in the future with data from new satellite  
372 missions like SBG.

373

374

375

376

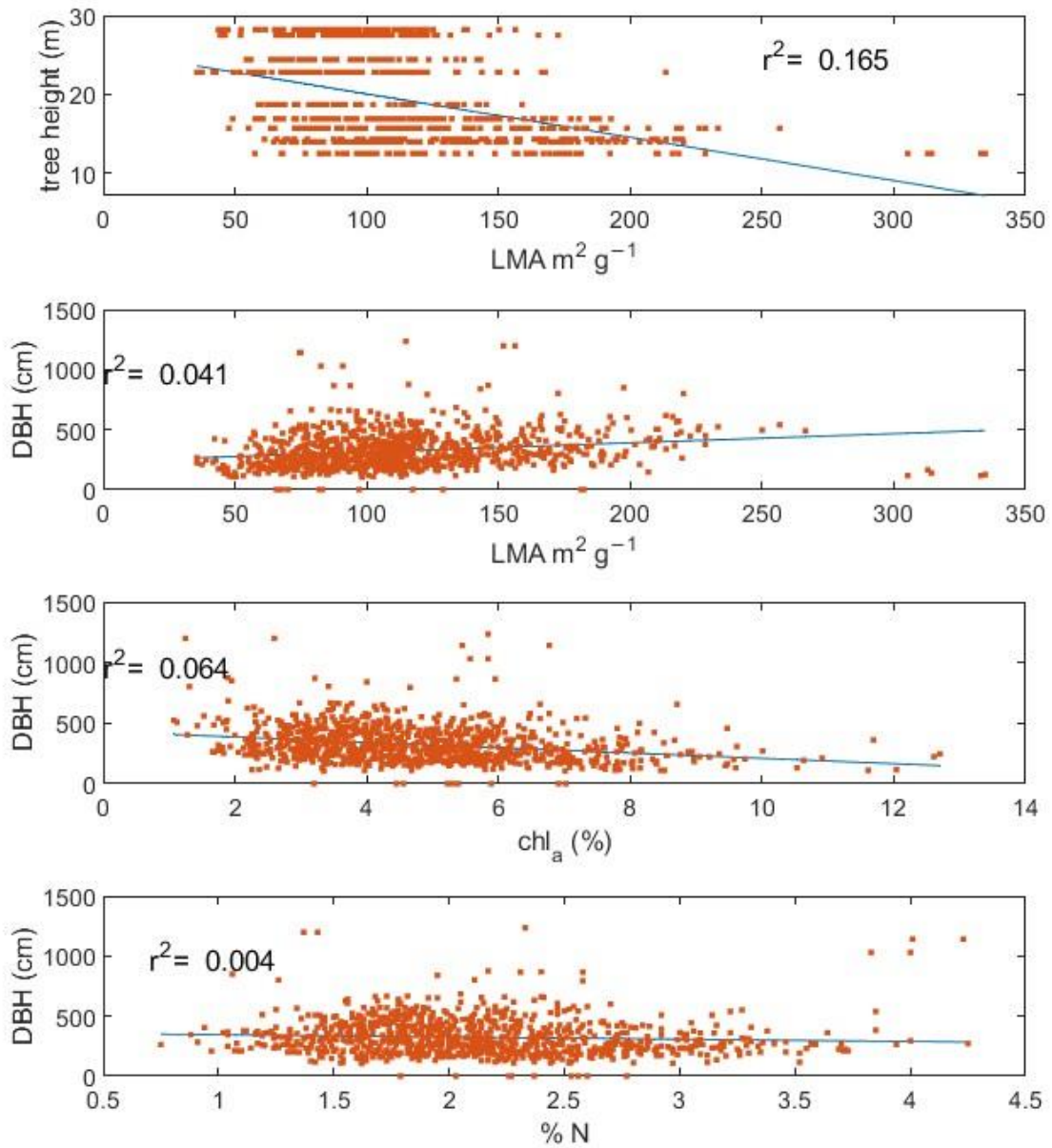
377 **Table 1** – Model results ( $\Delta AIC$  and adjusted  $R^2$ ) for field derived biomass, and GEDI predicted  
 378 biomass using GEDI measured forest height, GEDI measured maximum PAVD height, % one  
 379 peak, and leaf traits of LMA and % P. For  $\Delta AIC$  we give the change in  $\Delta AIC$  between the best  
 380 model and the second-best model. The best model column gives the best model according to  
 381 AIC and the variable removed (bolded and italicized) for the next best model.

field derived biomass				RS biomass		
Variables	$\Delta AIC$	Best model	Adj $r^2$	$\Delta AIC$	Best model	Adj $r^2$
height, peak, P	1	height, P, <b><i>PEAK</i></b>	0.0356	1.5	height, peak, <b><i>P</i></b>	0.799
height, peak, LMA		height, peak	0.0281		height, peak	0.799
height, HOME, P	3	height, P, <b><i>HOME</i></b>	0.0368	22	height, HOME, <b><i>P</i></b>	0.795
height, HOME, LMA	2	height,HOME, <b><i>LMA</i></b>	0.0326	7	height, HOME, <b><i>LMA</i></b>	0.793
height	-		0.0272	-		0.787

382

383

384 **Figures**

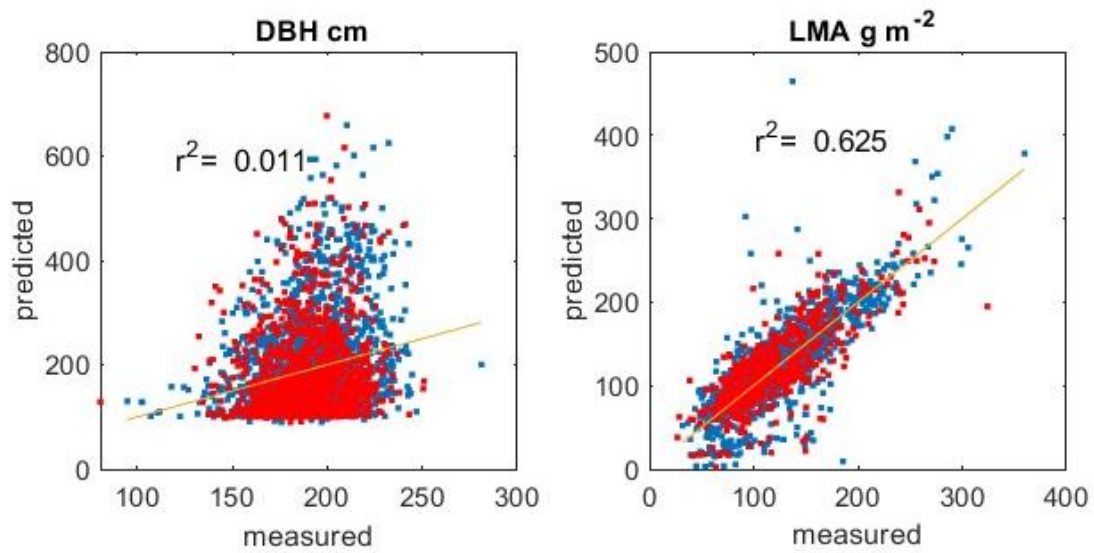


385

386 **Fig 1** –Individual tree DBH compared with leaf LMA (top), Chlorophyll A (middle) and % N  
387 (bottom), averaged on ~3 branches and 5 leaves per branch.

388

389



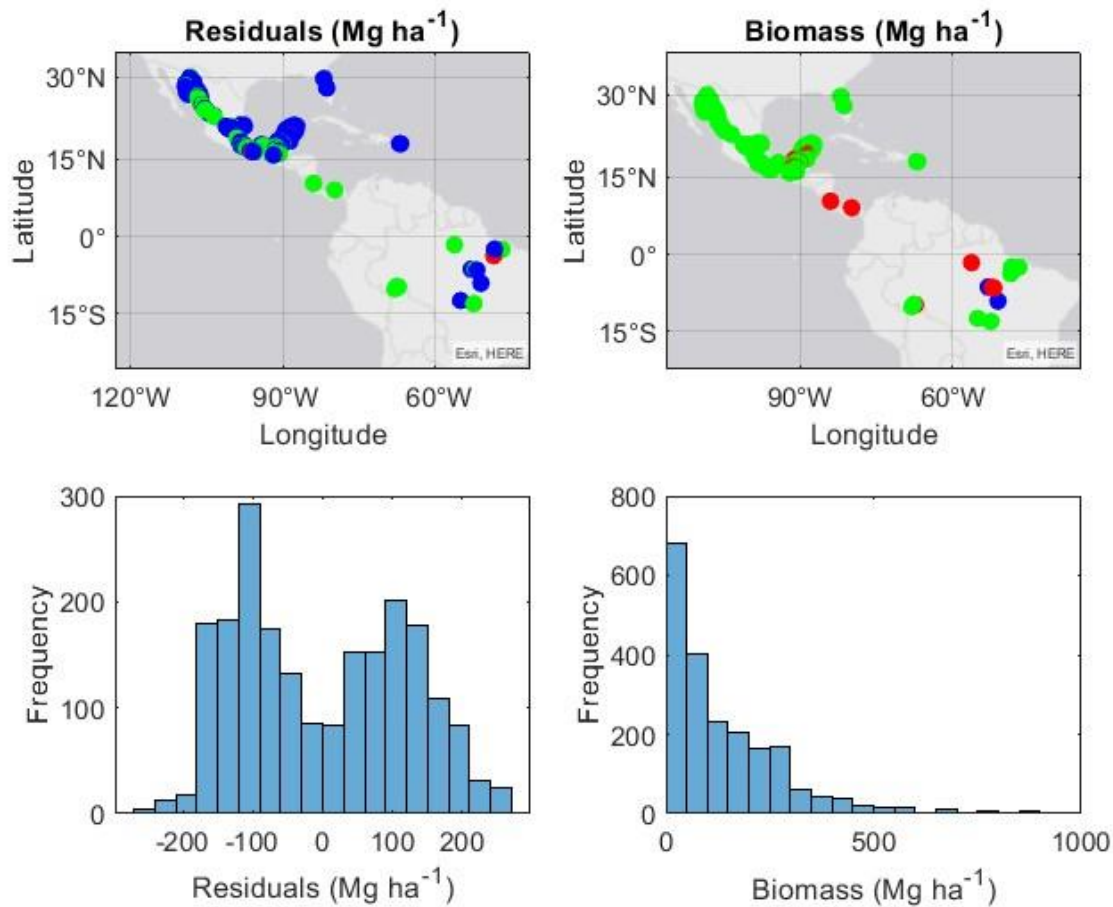
390

391 **Fig 2** –Leaf spectral (400-1075 nm) (N= 4690 individual leaves) averaged on ~3 branches and 5  
392 leaves per branch versus their diameter at Breast Height (DBH) (left) or Leaf Mass Area (LMA)  
393 (right) using the PLSR technique (blue is training data and red is the validation data).

394

395

396

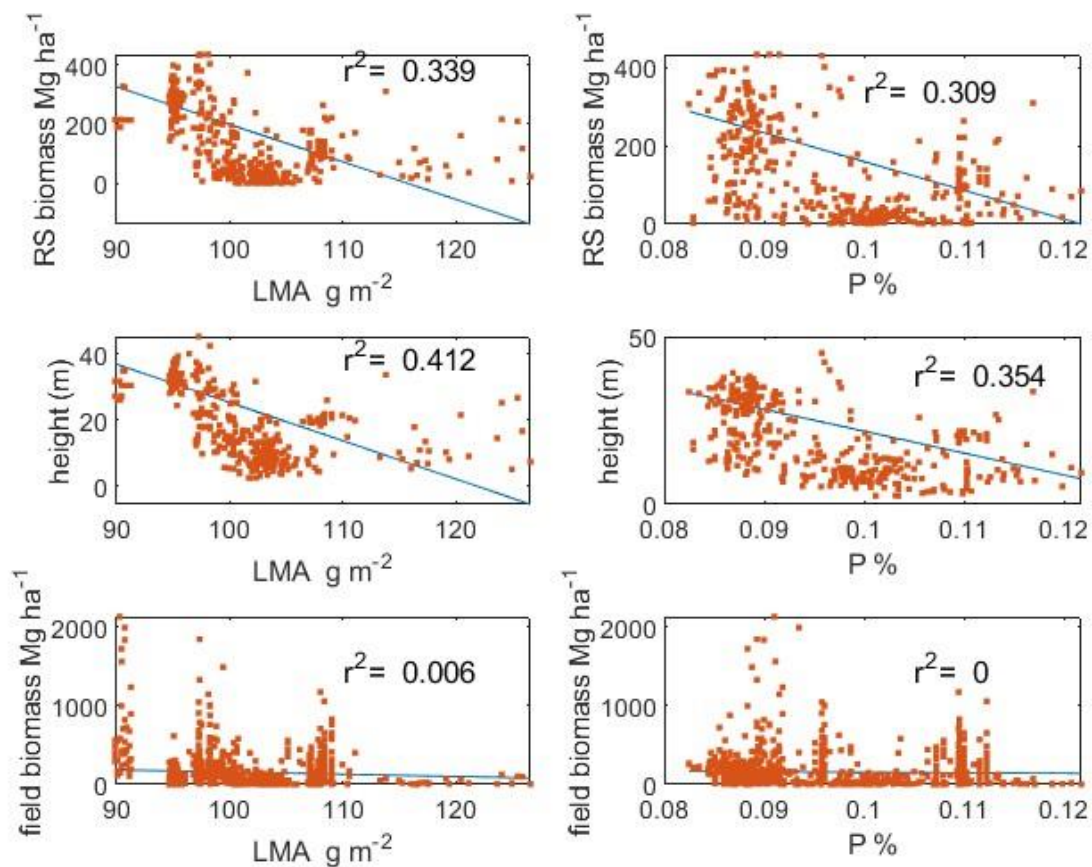


397

398 **Fig 3**—GEDI predicted biomass minus field biomass (residuals) (left) and field biomass (right)  
399 where (top) the color dots represents the value (residuals  $\text{Mg ha}^{-1}$  between 100 and -100 = green,  
400  $>100$  = red, and  $<-100$  blue and  $\text{AGB Mg ha}^{-1} < 150$ =green, between 150 and 300 = red and  
401  $>300$  = blue). For the maps we show a subset of the data for visual clarity. The full maps are  
402 shown in fig S1 and S2. On the bottom, we show a histogram of the residuals (left) and field  
403 biomass (right). All comparisons were aggregated to 300 by 300 m areas.

404

405



406

407 **Fig 4** – RS biomass (top), tree height (middle), and field derived biomass (bottom) versus remote  
408 sensed derived leaf traits LMA (left) and leaf % P (right).

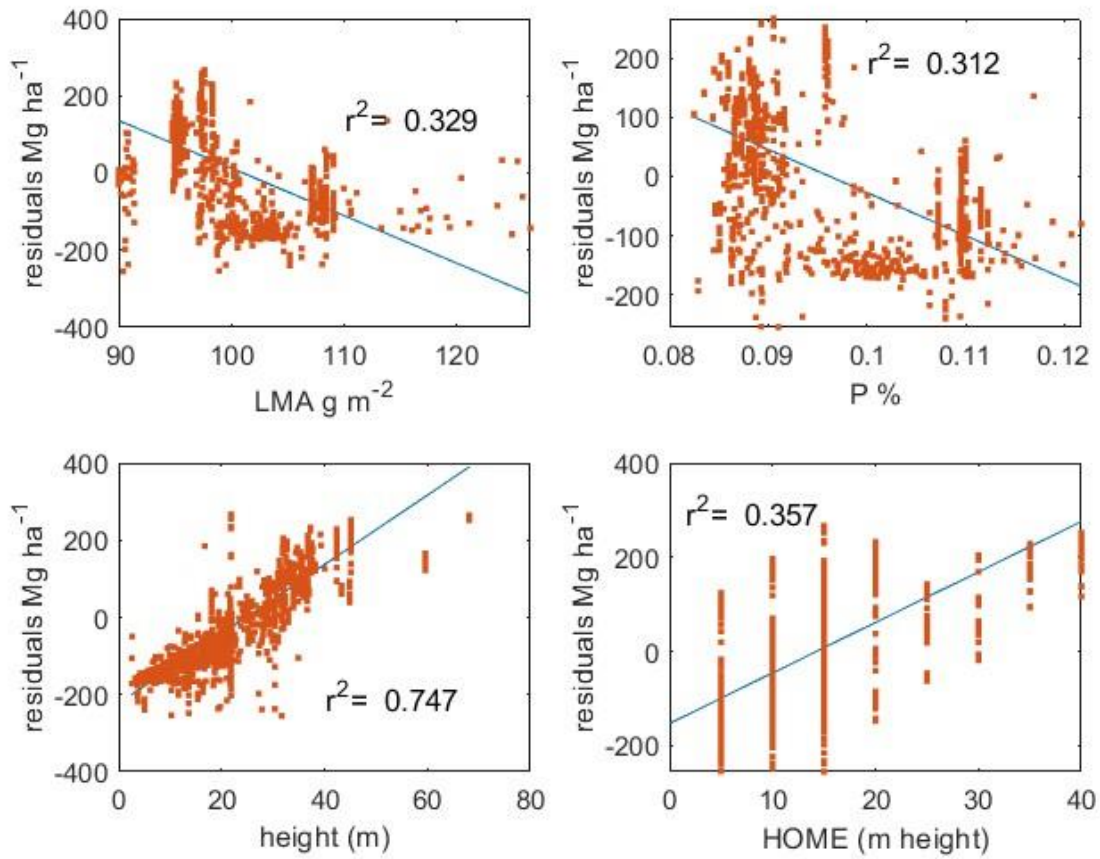
409

410

411

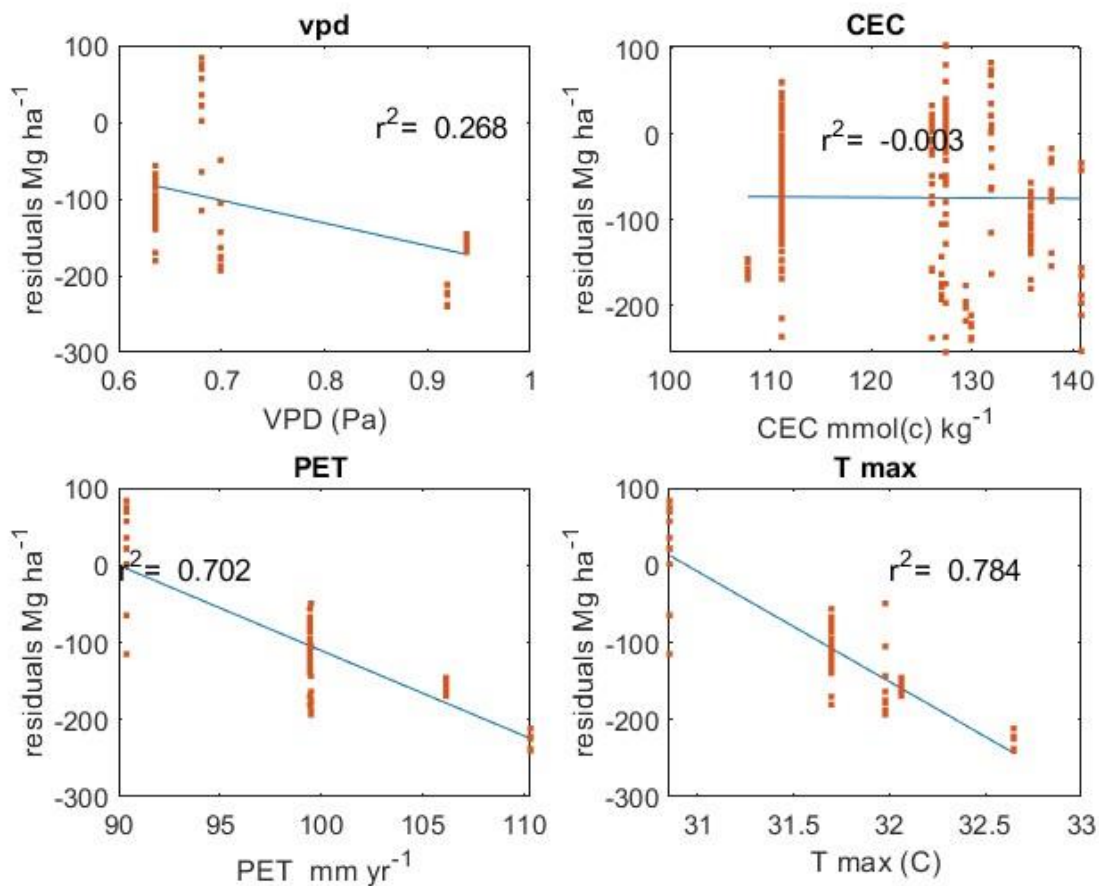
412





413

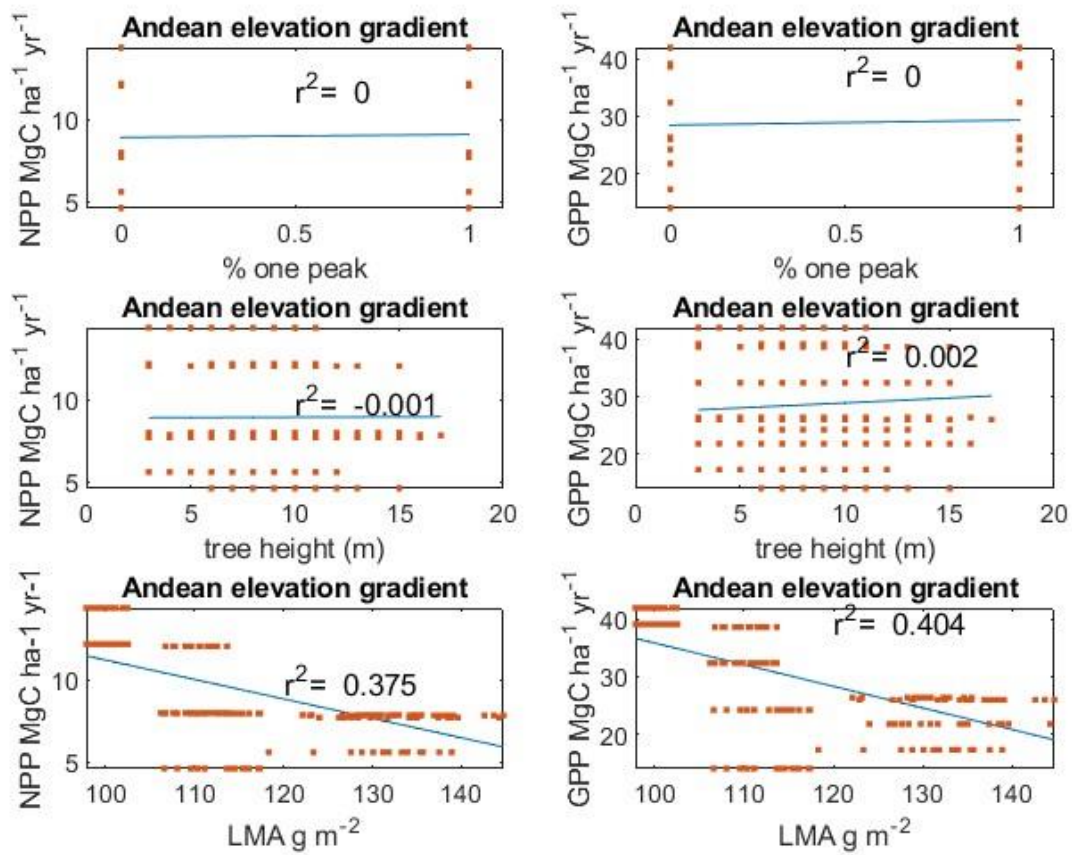
414 **Fig 5** – Biomass residuals (plot biomass minus GEDI predicted biomass) versus remotely sensed  
 415 leaf traits (P and LMA) and GEDI predicted structural variables (height and HOME).



416

417 **Fig 6** –Biomass residuals (plot biomass minus GEDI predicted biomass) versus soils (cation  
 418 exchange capacity - CEC) and climate data (vapor pressure deficit (VPD), potential  
 419 evapotranspiration (PET), and maximum temperature (T<sub>max</sub>).

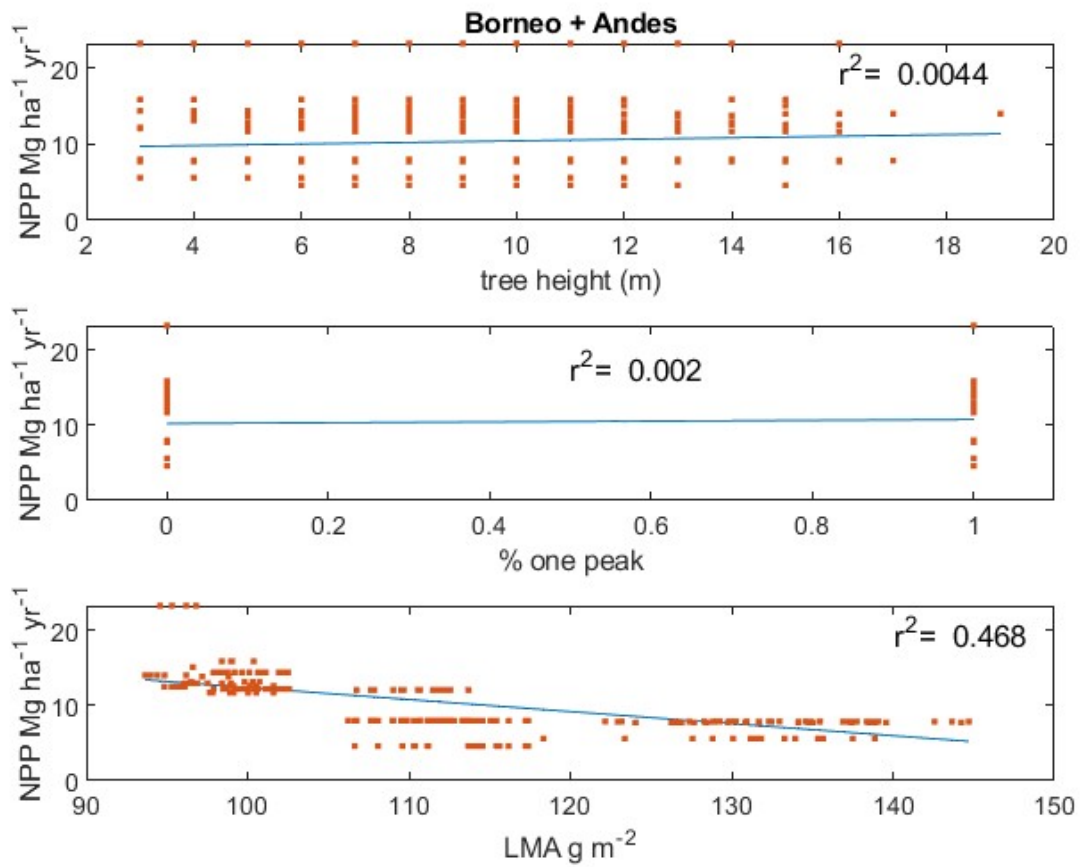
420



421

422 **Fig 7** – Net Primary Production (left) and Gross primary production (right) data from South  
 423 America compared to % one peak (top) with 1 = more than one peak and 0 = one peak, GEDI  
 424 calculated tree height (middle), and remote sensed LMA (bottom). GEDI data are from the  
 425 nearest 0.03 degrees pixel.

426



427

428 **Fig 8** – Net Primary Production data from Borneo and South America compared to GEDI  
 429 calculated tree height (top), % one peak (middle) (with 1 = more than one peak and 0 = one  
 430 peak) and remote sensed LMA (bottom).

431

432

433 References

- 434 Abatzoglou, J. T., Dobrowski, S. Z., Parks, S. A., & Hegewisch, K. C. (2018). TerraClimate, a  
 435 high-resolution global dataset of monthly climate and climatic water balance from 1958–  
 436 2015. *Scientific Data*, 5(1), 170191. <https://doi.org/10.1038/sdata.2017.191>
- 437 Aguirre-Gutiérrez, J., Rifai, S., Shenkin, A., Oliveras, I., Bentley, L. P., Svátek, M., et al. (2021).  
 438 Pantropical modelling of canopy functional traits using Sentinel-2 remote sensing data.  
 439 *Remote Sensing of Environment*, 252, 112122.  
 440 <https://doi.org/https://doi.org/10.1016/j.rse.2020.112122>
- 441 Asner, G. P., & Martin, R. E. (2008). Spectral and chemical analysis of tropical forests: Scaling  
 442 from leaf to canopy levels. *Remote Sensing of Environment*.  
 443 <https://doi.org/10.1016/j.rse.2008.07.003>
- 444 Asner, G. P., Knapp, D. E., Anderson, C. B., Martin, R. E., & Vaughn, N. (2016). Large-scale  
 445 climatic and geophysical controls on the leaf economics spectrum. *Proceedings of the*  
 446 *National Academy of Sciences of the United States of America*.  
 447 <https://doi.org/10.1073/pnas.1604863113>
- 448 Avitabile, V., Herold, M., Heuvelink, G. B. M., Lewis, S. L., Phillips, O. L., Asner, G. P., et al.  
 449 (2016). An integrated pan-tropical biomass map using multiple reference datasets. *Global*  
 450 *Change Biology*, 22(4), 1406–1420. <https://doi.org/https://doi.org/10.1111/gcb.13139>
- 451 Baccini, A., Goetz, S. J., Walker, W. S., Laporte, N. T., Sun, M., Sulla-Menashe, D., et al.  
 452 (2012). Estimated carbon dioxide emissions from tropical deforestation improved by  
 453 carbon-density maps. *Nature Climate Change*, 2(3), 182–185.  
 454 <https://doi.org/10.1038/nclimate1354>
- 455 Baret, F., Vanderbilt, V. C., Steven, M. D., & Jacquemoud, S. (1994). Use of spectral analogy to  
 456 evaluate canopy reflectance sensitivity to leaf optical properties. *Remote Sensing of*  
 457 *Environment*, 48(2), 253–260. [https://doi.org/https://doi.org/10.1016/0034-4257\(94\)90146-](https://doi.org/https://doi.org/10.1016/0034-4257(94)90146-5)  
 458 5
- 459 Bartoń, K. (2009). MuMIn: Multi-model inference. *R Package Version 0.12.2* .
- 460 Batjes, N. H., Ribeiro, E., & van Oostrum, A. (2020). Standardised soil profile data to support  
 461 global mapping and modelling (WoSIS snapshot 2019). *Earth System Science Data*, 12(1),  
 462 299–320. <https://doi.org/10.5194/essd-12-299-2020>
- 463 Cawse-Nicholson, K., Townsend, P. A., Schimel, D., Assiri, A. M., Blake, P. L., Buongiorno, M.  
 464 F., et al. (2021). NASA’s surface biology and geology designated observable: A perspective  
 465 on surface imaging algorithms. *Remote Sensing of Environment*, 257, 112349.  
 466 <https://doi.org/https://doi.org/10.1016/j.rse.2021.112349>
- 467 Clark, D. A., Piper, S. C., Keeling, C. D., & Clark, D. B. (2003). Tropical rain forest tree growth  
 468 and atmospheric carbon dynamics linked to interannual temperature variation during 1984–  
 469 2000. *Proceedings of the National Academy of Sciences*, 100(10), 5852–5857.  
 470 <https://doi.org/10.1073/pnas.0935903100>
- 471 Cleveland, C. C., Taylor, P., Chadwick, K. D., Dahlin, K., Doughty, C. E., Malhi, Y., et al.  
 472 (2015). A comparison of plot-based satellite and Earth system model estimates of tropical

473 forest net primary production. *Global Biogeochemical Cycles*.  
474 <https://doi.org/10.1002/2014GB005022>

475 Díaz, S., Kattge, J., Cornelissen, J. H. C., Wright, I. J., Lavorel, S., Dray, S., et al. (2016). The  
476 global spectrum of plant form and function. *Nature*. <https://doi.org/10.1038/nature16489>

477 Doughty, C. E., Santos-Andrade, P. E., Goldsmith, G. R., Blonder, B., Shenkin, A., Bentley, L.  
478 P., et al. (2017). Can Leaf Spectroscopy Predict Leaf and Forest Traits Along a Peruvian  
479 Tropical Forest Elevation Gradient? *Journal of Geophysical Research: Biogeosciences*.  
480 <https://doi.org/10.1002/2017JG003883>

481 Doughty, C. E., Gaillard, C., Burns, P., Keany, J. M., Abraham, A. J., Malhi, Y., et al. (2023).  
482 Tropical forests are mainly unstratified especially in Amazonia and regions with lower  
483 fertility or higher temperatures. *Environmental Research: Ecology*, 2(3), 35002.  
484 <https://doi.org/10.1088/2752-664X/ace723>

485 Dubayah, R., Blair, J. B., Goetz, S., Fatoyinbo, L., Hansen, M., Healey, S., et al. (2020). The  
486 Global Ecosystem Dynamics Investigation: High-resolution laser ranging of the Earth's  
487 forests and topography. *Science of Remote Sensing*.  
488 <https://doi.org/10.1016/j.srs.2020.100002>

489 Dubayah, R., Armston, J., Healey, S. P., Bruening, J. M., Patterson, P. L., Kellner, J. R., et al.  
490 (2022). GEDI launches a new era of biomass inference from space. *Environmental*  
491 *Research Letters*, 17(9), 95001. <https://doi.org/10.1088/1748-9326/ac8694>

492 Dubayah, R. O., Armston, J., Healey, S. P., Yang, Z., Patterson, P. L., Saarela, S., et al. (2023).  
493 GEDI L4B Gridded Aboveground Biomass Density, Version 2.1. ORNL Distributed Active  
494 Archive Center. <https://doi.org/10.3334/ORNLDAAC/2299>

495 Duncanson, L., Kellner, J. R., Armston, J., Dubayah, R., Minor, D. M., Hancock, S., et al.  
496 (2022). Aboveground biomass density models for NASA's Global Ecosystem Dynamics  
497 Investigation (GEDI) lidar mission. *Remote Sensing of Environment*, 270, 112845.  
498 <https://doi.org/https://doi.org/10.1016/j.rse.2021.112845>

499 Enquist, B. J., Bentley, L. P., Shenkin, A., Maitner, B., Savage, V., Michaletz, S., et al. (2017).  
500 Assessing trait-based scaling theory in tropical forests spanning a broad temperature  
501 gradient. *Global Ecology and Biogeography*, 26(12), 1357–1373.  
502 <https://doi.org/https://doi.org/10.1111/geb.12645>

503 F. Dormann, C., M. McPherson, J., B. Araújo, M., Bivand, R., Bolliger, J., Carl, G., et al. (2007).  
504 Methods to account for spatial autocorrelation in the analysis of species distributional data:  
505 a review. *Ecography*, 30(5), 609–628. <https://doi.org/https://doi.org/10.1111/j.2007.0906-7590.05171.x>

507 Fox J, & S, W. (2019). *An R Companion to Applied Regression*.

508 Geladi, P., & Kowalski, B. R. (1986). Partial least-squares regression: a tutorial. *Analytica*  
509 *Chimica Acta*. [https://doi.org/10.1016/0003-2670\(86\)80028-9](https://doi.org/10.1016/0003-2670(86)80028-9)

510 Goetz, S. J., Hansen, M., Houghton, R. A., Walker, W., Laporte, N., & Busch, J. (2015).  
511 Measurement and monitoring needs, capabilities and potential for addressing reduced  
512 emissions from deforestation and forest degradation under REDD+. *Environmental*

513 *Research Letters*, 10(12), 123001. <https://doi.org/10.1088/1748-9326/10/12/123001>

514 Gorman, E. T., Kubalak, D. A., Patel, D., Dress, A., Mott, D. B., Meister, G., & Werdell, P. J.  
515 (2019). The NASA Plankton, Aerosol, Cloud, ocean Ecosystem (PACE) mission: an  
516 emerging era of global, hyperspectral Earth system remote sensing. In *Proc.SPIE* (Vol.  
517 11151, p. 111510G). <https://doi.org/10.1117/12.2537146>

518 Halle, F., Oldeman, R., & Tomlinson, P. (1980). *Tropical Trees and Forests: An Architectural*  
519 *Analysis*. New York: Springer.

520 Hancock, S., Armston, J., Hofton, M., Sun, X., Tang, H., Duncanson, L. I., et al. (2019). The  
521 GEDI Simulator: A Large-Footprint Waveform Lidar Simulator for Calibration and  
522 Validation of Spaceborne Missions. *Earth and Space Science*, 6(2), 294–310.  
523 <https://doi.org/https://doi.org/10.1029/2018EA000506>

524 Homolová, L., Malenovský, Z., Clevers, J. G. P. W., García-Santos, G., & Schaepman, M. E.  
525 (2013). Review of optical-based remote sensing for plant trait mapping. *Ecological*  
526 *Complexity*, 15, 1–16. <https://doi.org/https://doi.org/10.1016/j.ecocom.2013.06.003>

527 Malhi, Y., Girardin, C. A. J., Goldsmith, G. R., Doughty, C. E., Salinas, N., Metcalfe, D. B., et  
528 al. (2017). The variation of productivity and its allocation along a tropical elevation  
529 gradient: a whole carbon budget perspective. *New Phytologist*, 214(3), 1019–1032.  
530 <https://doi.org/https://doi.org/10.1111/nph.14189>

531 Malhi, Y., Girardin, C., Metcalfe, D. B., Doughty, C. E., Aragão, L. E. O. C., Rifai, S. W., et al.  
532 (2021). The Global Ecosystems Monitoring network: Monitoring ecosystem productivity  
533 and carbon cycling across the tropics. *Biological Conservation*, 253, 108889.  
534 <https://doi.org/https://doi.org/10.1016/j.biocon.2020.108889>

535 Mitchard, E. T. A., Saatchi, S. S., Baccini, A., Asner, G. P., Goetz, S. J., Harris, N. L., & Brown,  
536 S. (2013). Uncertainty in the spatial distribution of tropical forest biomass: a comparison of  
537 pan-tropical maps. *Carbon Balance and Management*, 8(1), 10.  
538 <https://doi.org/10.1186/1750-0680-8-10>

539 Mitchard, E. T. A., Feldpausch, T. R., Brienen, R. J. W., Lopez-Gonzalez, G., Monteagudo, A.,  
540 Baker, T. R., et al. (2014). Markedly divergent estimates of Amazon forest carbon density  
541 from ground plots and satellites. *Global Ecology and Biogeography*, 23(8), 935–946.  
542 <https://doi.org/https://doi.org/10.1111/geb.12168>

543 Réjou-Méchain, M., Mortier, F., Bastin, J.-F., Cornu, G., Barbier, N., Bayol, N., et al. (2021).  
544 Unveiling African rainforest composition and vulnerability to global change. *Nature*,  
545 593(7857), 90–94. <https://doi.org/10.1038/s41586-021-03483-6>

546 Riutta, T., Malhi, Y., Kho, L. K., Marthews, T. R., Huaraca Huasco, W., Khoo, M., et al. (2018).  
547 Logging disturbance shifts net primary productivity and its allocation in Bornean tropical  
548 forests. *Global Change Biology*, 24(7), 2913–2928. <https://doi.org/10.1111/gcb.14068>

549 Saatchi, S. S., Harris, N. L., Brown, S., Lefsky, M., Mitchard, E. T. A., Salas, W., et al. (2011).  
550 Benchmark map of forest carbon stocks in tropical regions across three continents.  
551 *Proceedings of the National Academy of Sciences*, 108(24), 9899–9904.  
552 <https://doi.org/10.1073/pnas.1019576108>

- 553 Schimel, D. S., & Poulter, B. (2022). The Earth in Living Color - NASA's Surface Biology and  
554 Geology Designated Observable. In *2022 IEEE Aerospace Conference (AERO)* (pp. 1–6).  
555 <https://doi.org/10.1109/AERO53065.2022.9843640>
- 556 ter Steege, H., Pitman, N. C. A., Phillips, O. L., Chave, J., Sabatier, D., Duque, A., et al. (2006).  
557 Continental-scale patterns of canopy tree composition and function across Amazonia.  
558 *Nature*, *443*(7110), 444–447. <https://doi.org/10.1038/nature05134>
- 559 Stovall, A. E. L., & Shugart, H. H. (2018). Improved Biomass Calibration and Validation With  
560 Terrestrial LiDAR: Implications for Future LiDAR and SAR Missions. *IEEE Journal of*  
561 *Selected Topics in Applied Earth Observations and Remote Sensing*, *11*(10), 3527–3537.  
562 <https://doi.org/10.1109/JSTARS.2018.2803110>
- 563 Tuomisto, H., Van doninck, J., Ruokolainen, K., Moulatlet, G. M., Figueiredo, F. O. G., Sirén,  
564 A., et al. (2019). Discovering floristic and geocological gradients across Amazonia.  
565 *Journal of Biogeography*, *46*(8), 1734–1748.  
566 <https://doi.org/https://doi.org/10.1111/jbi.13627>
- 567 Ustin, S. L., Asner, G. P., Gamon, J. A., Fred Huemmrich, K., Jacquemoud, S., Schaepman, M.,  
568 & Zarco-Tejada, P. (2006). Retrieval of quantitative and qualitative information about plant  
569 pigment systems from high resolution spectroscopy. In *International Geoscience and*  
570 *Remote Sensing Symposium (IGARSS)*. <https://doi.org/10.1109/IGARSS.2006.517>
- 571 Zhang, F., Chen, J. M., Chen, J., Gough, C. M., Martin, T. A., & Dragoni, D. (2012). Evaluating  
572 spatial and temporal patterns of MODIS GPP over the conterminous U.S. against flux  
573 measurements and a process model. *Remote Sensing of Environment*, *124*, 717–729.  
574 <https://doi.org/https://doi.org/10.1016/j.rse.2012.06.023>

575

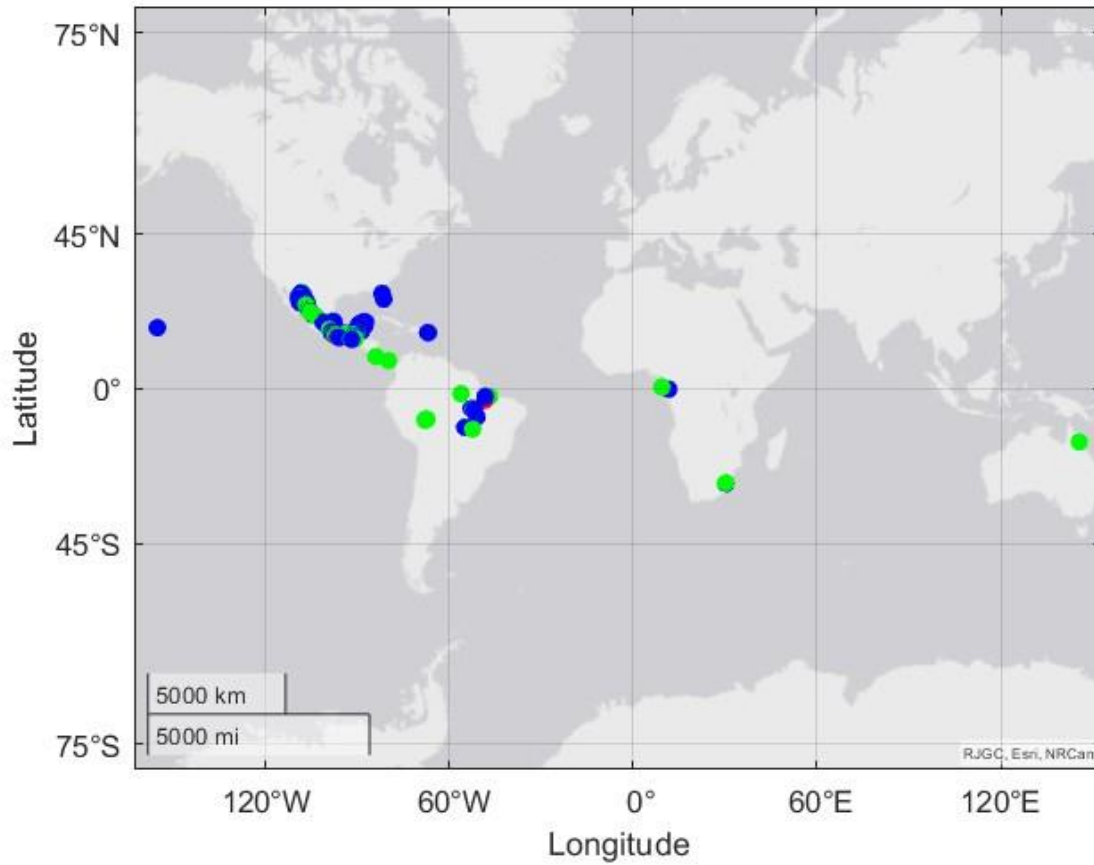
576



577 **Supplemental figures**

578

579



580

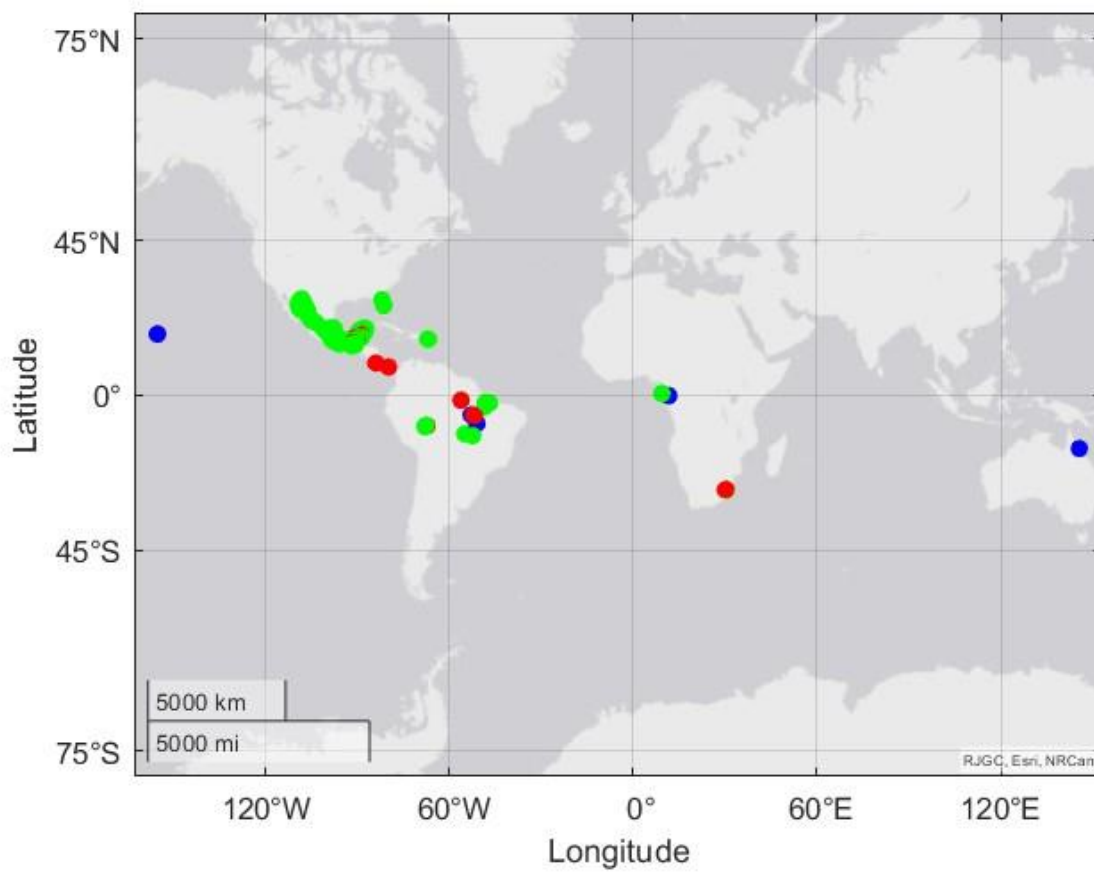
581

582 **Figure S1**—GEDI predicted biomass minus field biomass (residuals) where the color dots  
583 represents the value (residuals  $\text{Mg ha}^{-1}$  between 100 and -100 = green,  $>100$  = red, and  $<-100$   
584 blue.

585

586

587

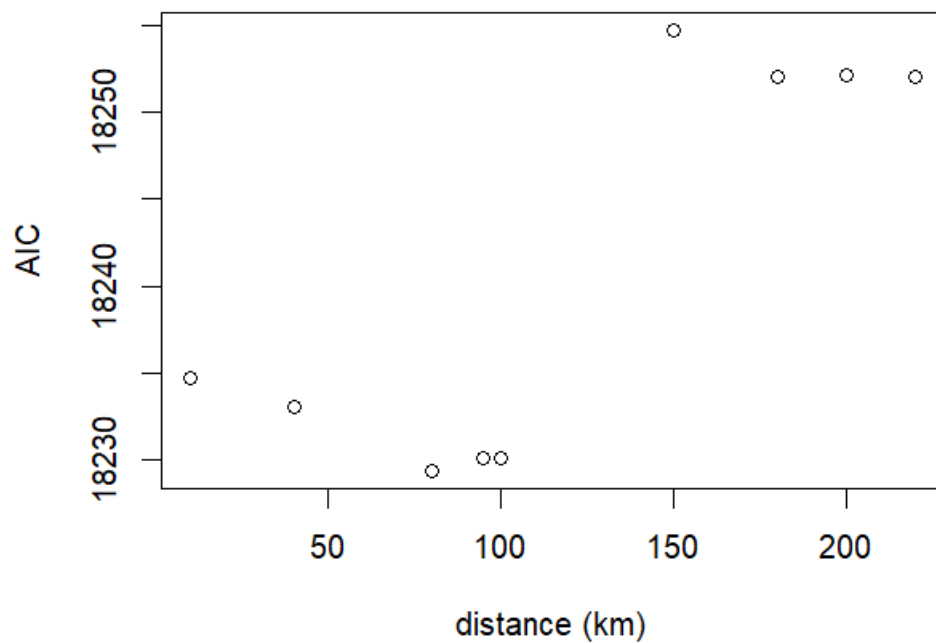


588

589 **Figure S2**–Field biomass where the color dots represent the value AGB Mg ha<sup>-1</sup> (< 150=green,  
 590 between 150 and 300 = red and >300 = blue).

591

592

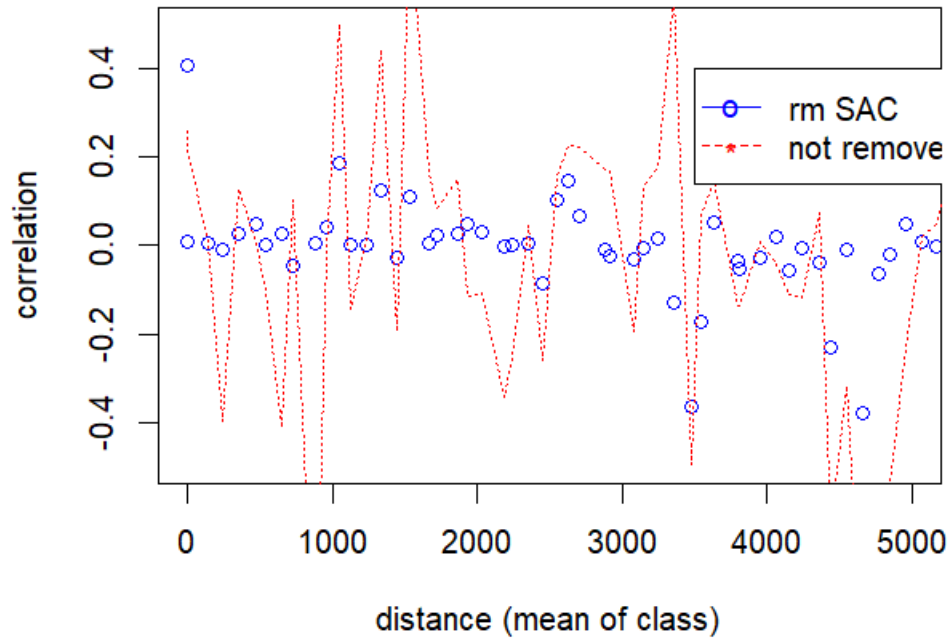


593

594

595 **Figure S3** –Comparing model AIC to radius (km) to average data showing a reduced AIC value  
596 with a neighborhood distance of 80km model for a model using height, bulk, and LMA to predict  
597 field biomass.

598



599

600 **Figure S4** – Example Correlogram for model using height, bulk, and LMA to predict field  
 601 biomass with no neighborhood removing spatial autocorrelation (red dashed line) and for a  
 602 neighborhood of 80km (blue dots).

603